Toxicology in Vitro 31 (2016) 126–136

Contents lists available at ScienceDirect

Toxicology in Vitro

journal homepage: www.elsevier.com/locate/toxinvit

Polystyrene nanoparticles internalization in human gastric adenocarcinoma cells

Maurizio Forte [a,b], Giuseppina Iachetta [a], Margherita Tussellino [a], Rosa Carotenuto [a], Marina Prisco [a], Maria De Falco [a], Vincenza Laforgia [a], Salvatore Valiante [a,*]

[a] Department of Biology, University of Naples Federico II, Naples, Italy
[b] National Laboratory on endocrine disruptors (INBB), Institute of Genetics and Biophysics "A. Buzzati-Traverso," CNR, Naples, Italy

ARTICLE INFO

Article history:
Received 14 July 2015
Received in revised form 14 October 2015
Accepted 9 November 2015
Available online 14 November 2015

Keywords:
Nanoparticles uptake
Gastric cells
Endocytosis
Interleukins

ABSTRACT

The increase in the use of nanoparticles, as a promising tool for drug delivery or as a food additive, raises questions about their interaction with biological systems, especially in terms of evoked responses. In this work, we evaluated the kinetics of uptake of 44 nm (NP44) and 100 nm (NP100) unmodified polystyrene nanoparticles (PS-NPs) in gastric adenocarcinoma (AGS) cells, as well as the endocytic mechanism involved, and the effect on cell viability and gene expression of genes involved in cell cycle regulation and inflammation processes. We showed that NP44 accumulate rapidly and more efficiently in the cytoplasm of AGS compared to NP100; both PS-NPs showed an energy dependent mechanism of internalization and a clathrin-mediated endocytosis pathway. Dose response treatments revealed a non-linear curve. PS-NPs also affected cell viability, inflammatory gene expression and cell morphology. NP44 strongly induced an up-regulation of IL-6 and IL-8 genes, two of the most important cytokines involved in gastric pathologies. Our study suggests that parameters such as time, size and concentration of NPs must be taken carefully into consideration during the development of drug delivery systems based on NPs and for the management of nanoparticles associated risk factors.

1. Introduction

Nanoparticles (NPs) are defined as materials with dimension range between 1 and 100 nm (Beer et al., 2012). They are being used in several application fields, such as electronic, cosmetic, food industry and medicine (Dekkers et al., 2011; Osmond and McCall, 2010). In medicine, in particular, they are a promising tool both in diagnosis and therapy (Cuenca et al., 2006; Schlorf et al., 2011; Soriano et al., 2013; Wickline and Lanza, 2003). NPs can be engineered with proteins, gene segments or siRNA encapsulated inside them or attached to their surface (Cai and Xu, 2011; Ferrari, 2005; Mora-Huertas et al., 2010; Panyam and Labhasetwara, 2003). On the other side, NPs can be accumulated in the environment and may be responsible for human pathologies when inhaled or ingested (Boczkowski and Hoet, 2010; Boraschi et al., 2012; Shang et al., 2014). Thus, it's clear that the first step for the use of NPs based systems is to characterize their interaction with cells, especially in terms of toxicity and internalization pathways.

Molecules enter in cells through different mechanisms of internalization: the most characterized are clathrin-dependent and clathrin independent pathways, such as macropinocytosis and phagocytosis (Bareford and Swaan, 2007). Briefly, in clathrin-mediated endocytosis, cells internalize molecules by the invagination of plasma membrane under the control of the small GTP-ase dynamin that is required for the budding of vesicles inside the cell. Typical size range of clathrin coated-pits is reported to be 60–200 nm (Rejman et al., 2004; Kirchhausen et al., 2008). Phagocytosis is mediated by Rho family GTP-ases that trigger the polymerization of actin at the site of ingestion to form membrane invagination that then culminate in the formation of phagolysosome. Although this process is typical of some cells, it is well known that also non-specialized cells in rare situations can activate phagocytosis (Gagnon et al., 2002). Macropinocytosis involves the internalization of various area of plasma membrane that lead to the formation of vesicle of approximately 150 nm of size (dos Santos et al., 2011). This invagination depends, in the same way of phagocytosis, by actin rearrangements, triggered by Rho-family GTP-ase (Mercer and Helenius, 2009).

In our study we used polystyrene nanoparticles (PS-NPs), that represent an interesting model to study interactions between NPs and cells for some practical reasons: first, they are commercially available and can be obtained in core-labeled fluorescent form allowing localization and tracking in living cells (Varela et al., 2012); second, they can be synthesized in a wide range of sizes or easily modified on their surface

Abbreviations: NPs, nanoparticles; PS-NPs, polystyrene nanoparticles; EIPA, 5-(N-ethyl-N-isopropyl) amiloride; NP100, 100 nm rhodamine polystyrene nanoparticles (PS-NPs); NP44, 44 nm fluorescein isothiocyanate polystyrene nanoparticles (PS-NPs); MTT, 3-[4,5-dimethylthiazol-2-yl]-3,5 diphenyltetrazolium bromide test; IL, interleukins.

* Corresponding author at: 8, Via Mezzocannone, 80134 Naples, Italy.
E-mail address: valiante@unina.it (S. Valiante).

http://dx.doi.org/10.1016/j.tiv.2015.11.006
0887-2333/

(Lunov et al., 2011); third, they have a high drug loading capacity and a colloidal stability in biological media (Holzapfel et al., 2005; Musyanovych et al., 2007). For these characteristics, there are many studies on the interactions between PS-NPs and cell lines; these studies were performed in the presence or in the absence of specific pharmacological inhibitors of endocytosis pathways. PS-NPs have been reported to enter in different cell types such as hepatocytes (Johnston et al., 2010), macrophages (Xia et al., 2008), lung cells (Geys et al., 2006) and glial astrocytoma cells (dos Santos et al., 2011). Results from these studies showed that parameters that govern the *in vitro* mechanism of internalization and the uptake rates of PS-NPs are the cell type, NPs shape and size, as well as the presence or absence of serum in the cell medium (Guarnieri et al., 2011; Smith et al., 2012). In this paper, we investigated the toxicity and the cellular uptake of fluorescent labeled PS-NPs of two representative sizes (44 nm and 100 nm) in human gastric adenocarcinoma (AGS) cell line: we chose human gastric cells since it has been accepted that for humans one of the primary route of contact with NPs is the ingestion of contaminated food, such as plant derivates (Nowack and Bucheli, 2007) and that huge amounts of PS-NPs reach, through the food chain, fish (Cedervall et al., 2012) with severe consequences on their metabolism and behavior (Mattsson et al., 2014), thus making conceivable the potential contact with human tissues through the alimentation. Both clathrin-mediated and caveolin-mediated endocytosis were studied using the dynamin inhibitor dynasore (Macia et al., 2006) while for clathrin independent pathways the selective Na^+/H^+ antiporter inhibitor 5-(N-ethyl-N-isopropyl) amiloride (EIPA) was used (Lagana et al., 2000). We demonstrated the efficiency of the internalization process, the amount of PS-NP uptake, internal cluster arrangement, the effect on cell viability and changing of gene expression of some genes involved in cell cycle and inflammation responses.

2. Materials and methods

2.1. Cell culture

Human gastric adenocarcinoma epithelial cells (AGS, American Type Culture Collection CRL1739, Manassan, VA) were grown in Dulbecco's Modified Eagle's medium (DMEM) (LONZA), supplemented with 10% fetal bovine serum (FBS), 2 mm L-glutamine and antibiotics (100 U/ml penicillin/streptomycin, 10 μg/ml gentamicin) in a humidified incubator at 37 °C and 5% CO_2. When confluent, the cell line was detached enzymatically with trypsin-ethylenediamine tetra-acetic acid (Trypsin–EDTA) and subcultured into a new cell culture flask. The medium was replaced every 2 days. Cells were used for experiments between passages 15–25.

2.2. Nanoparticle characterization and chemicals

100 nm rhodamine PS-NPs (NP100) and 44 nm fluorescein isothiocyanate PS-NPs (NP44) unmodified polystyrene nanoparticles (PS-NPs) were purchased from Duke scientific corporation (Palo Alto, CA, USA) and used without further modifications (Table 1). Dynamic light scattering (DLS), made with a Zetasizer Nano-ZS (Malvern Instruments, Worcestershire, UK), was performed to measure PS-NPs size distribution, z-potential and polydispersity index (PdI) which is the value that indicates whether the distribution in the size of NP is more or less homogeneous. PdI values less than 0.2 indicate homogeneous distribution of PS-NPs in the solution. Measures were conducted at 25 °C and 37 °C, without sonication, using 10 μg/ml PS-NPs in DMEM or in H_2O. The nanoparticles were suspended in DMEM at concentration of 5 mg/ml and after 1 h were diluted to 10 μg/ml for measurement in the ZetaSizer (Fröhlichet al., 2012).

Determination of size and z-potential was performed in triplicate and every value represents the mean of five measures. NP dispersions were prepared by diluting the concentrated stock solutions into the serum-free medium used for cell culture, at room temperature, with or without inhibitor drugs, immediately prior to the experiments on cells, with an identical time delay between diluting and introducing to the cells for all experiments. The medium was kept at room temperature and not pre-warmed to 37 °C to ensure better NP dispersions. Before sampling, NPs were vigorously mixed by vortexing. For inhibition studies two different drugs were used in the following final concentration: dynasore (25.8 μg/ml) for clathrin-dependent pathways and 5-(N-ethyl-N-isopropyl) amiloride (EIPA) (30 μg/ml) for macropinocytosis/phagocytosis (both from Sigma). Concentration used for inhibitor drugs refers to the work of Daunsend et al. (2008) for HeLa cells. All experiments were performed in the dark. To assess the efficacy of inhibitor drugs, transferrin and dextran were used as positive control, for clathrin dependent and independent pathways, respectively (data not showed).

2.3. Fluorescence microscopy

For fluorescence microscopy 5×10^4 AGS cells were allowed to attach in 4-well chamber slide overnight. The following day, cells were incubated with 10 μg/ml nanoparticle dispersions in serum-free medium (1 h at 37 °C). After the incubation time, cells were rinsed twice with PBS, in order to eliminate non-internalized PS-NPs and then fixed for 5 min with 4% paraformaldehyde in PBS. Cell nuclei were counterstained with Höechst 33258 (1 μg/ml). Inhibition studies were assessed for 1 h after pre-treatment for 30 min with dynasore and EIPA. Fluorescent images were taken on an Axioskop (Carl Zeiss) epi-fluorescence microscope using a 40× (NA = 0.75) and 100× oil immersed (NA = 1.3) objectives. Axiocam MRc5 and the acquisition software Axiovision 4.7 (Carl Zeiss) were used to capture the images in three different channels: Rhodamine for NP100 (ex: 580 nm; em: 605 nm), FITC for NP44 (ex: 488 nm; em: 535 nm) and Höechst 33258 for nuclei (ex: 350 nm; em: 461 nm). Three independent experiments were performed for each experimental condition and different fields were randomly chosen for data analysis.

2.4. Spectrofluorimetric assays

To evaluate the ability to internalize PS-NPs both dose and time course were evaluated. The time course was performed using 1×10^5 cells/well seeded in white bottom 96 multiwell. At 24 h post-seeding, cells were incubated with PS-NPs at the final concentration of 10 μg/ml in DMEM serum free for different times (1 min, 10 min,

Table 1
Chemical features of polystyrene nanoparticles (PS-NPs).

NPs	Composition	Concentration	Contents	Diameter (metric) mean	Diameter (metric) nominal	Dye type	Particle density	particle size	Uniformity	Refractive index
PS-NPs44 nm	Polystyrene	1% solids	Dyed polystyrene microspheres in water	0.04 μm	0.04 μm	Firefli™ fluorescent green (468/508 nm)	1.05 g/cm^3	0.04 μm	<15%	1.59 at 589 nm (25 °C)
PS-NPs 100 nm	Polystyrene	1% solids	Dyed polystyrene microspheres in water	0.10 μm	0.10 μm	Firefli™ fluorescent red (542/612 nm)	1.05 g/cm^3	0.10 μm	<10%	1.59 at 589 nm (25 °C)

20 min, 30 min, 60 min). For the 4 °C experiments, cells were put on ice for 15 min before adding PS-NPs. For inhibition studies, AGS cells were pre-treated with dynasore and EIPA for 30 min and inhibition was performed for a period of 1 h. After the incubation period, cells were rinsed twice with PBS for 5 min and then lysed with 200 μl/well of 1% Triton X-100 (Xiao et al., 2011) in order to release internalized nanoparticles. The dose course was performed seeding 1×10^5 cell/wells and adding 2, 5, 10, 20 and 30 μg/ml of each kind of PS-NPs. After 1 h supernatants were removed, cells washed three times with PBS and then 1% Triton X-100 used for cell lyses. Known amounts of PS-NPs were used to measure the maximum fluorescence and then used to express the fluorescence of samples as percentage of the corresponding amount. Fluorescence intensity was measured with a Tecan Infinite 200 microplate reader (Tecan) at excitation/emission wavelengths of 580/605 nm for NP100 and 485/535 nm for NP44. Calibration lines (data not showed) for both nanoparticles were performed in order to calculate the exact concentration of internalized nanoparticles. Spectrofluorimetric assays were performed in triplicate for each incubation time.

2.5. Image analysis of PS-NP distribution

PS-NPs detection for intracellular distribution was evaluated using 100×-oil immersed Plan-Neofluar objective with NA = 1.3 (Zeiss) mounted on Z axis piezo stage Nano-F200 controlled by Nano-Drive controller (Mad City Labs); images were acquired by Axiocam MRc5 at resolution of 2584 × 1936 (binning 1 × 1). The point spread function (PSF), calculated by measuring the FWHM of the profile of 100 nm fluorescent beads at the end of revelation path was of 240 nm in lateral resolution. To permit the evaluation of either single or aggregates of PS-NPs within AGS cells, images were acquired as z-stack and deconvolved (15 iterations) with the plug-in Deconvolution lab of ImageJ 1.48 (Vonesch and Unser, 2008); then the difference of Gaussian method was applied on deconvolved images, by the appropriate GDSC ImageJ plugin (http://www.sussex.ac.uk/gdsc/intranet/microscopy/imagej/toolsets). The σ_1 and σ_2 radius values applied were 5 and 1, respectively. Binarized spots allowed the application of the analyze particle plug-in to detect PS-NP aggregates inside cells (visualized as vertical lines along the z-axis in the 3D inserts of images) with the following parameter set: circularity ranging between 0.7 to 1.00 (1.00 = perfect circle), single pixel square size of at least of 1141 nm^2, and linear pixel size of 34 nm; this latter was within the appropriate right (100 nm × 100 nm) Nyquist sampling needed, calculated using the Nyquist Calculator (SVI, http://www.svi.nl/NyquistCalculator). The area of a single NP44 was approximately of 1520.53 nm^2 while NP100 of 7853.98 nm^2 hence both larger than the single pixel area. The distribution of the total number of NPs/μm^2 and the mean number of NPs/μm^2 aggregates inside cells was then calculated.

2.6. Morphological investigation

AGS cells were plated in 4-chamber slides and incubated for 24 h. Then PS-NPs samples with a final concentration of 10 μg/ml were added in the culture medium. Cells cultured in normal medium without PS-NPs were used as control. After 1 h, cells were washed twice with PBS and then soaked in methanol containing 1 μg/mL Höechst at 37 °C for 15 min. The cell morphology was observed under an epifluorescent microscope Axioskop (Carl Zeiss) and the ratio nucleus/cytoplasm was evaluated by ImageJ software 1.48.

2.7. Cell viability assay

The effects of nanoparticles on AGS viability were evaluated using the 3-[4,5-dimethylthiazol-2-yl]-3,5 diphenyltetrazolium bromide (MTT) test (Cayman Chemicals). Cells were seeded in 200 μl of growth medium (1×10^5 cells/well) in 96-well plates and pre-incubated for 24 h to recover. Then, 100 μl of freshly prepared nanoparticle dispersions in DMEM was added immediately after dilution to an appropriate concentration (10 μg/ml, 2 μg/ml, 1 μg/ml). After 24 h of incubation, 10 μl of a MTT solution was added to each well. After 4 h of 37 °C incubation, the culture medium was gently aspirated and replaced by 100 μl of Crystal dissolving solution in order to dissolve the formazan crystals. The absorbance of the solubilized dye, which correlates with the number of living cells, was measured with a microplate reader at 570 nm. The test was performed in triplicate.

2.8. RNA extraction, reverse transcription and real time PCR

Expression levels of mRNA of pro-inflammatory cytokines and genes of proliferation were analyzed using real-time PCR. Total RNA from control AGS and treated for 1 h with NP44 and NP100 (10 μg/ml), was extracted using the PureLink® RNA Mini Kit (Ambion, Life Technologies). Contaminating genomic DNA was removed by treatment with the TURBO DNA-free™ Kit (Ambion, Life Technologies) and the total amount of RNA was quantified with a NanoDrop spectrophotometer. cDNAs were synthesized from 1 μg RNA using the High Capacity cDNA Reverse Transcriptase (Life Technologies) and quantitative PCR was performed by using the 7500 Real-Time PCR System and SYBR® Select Master Mix 2X assay (Applied Biosystem, Courtaboeuf, France). All primers used were designed according to the sequences published on GenBank using Primer Express software version 3.0 (Table 3). The amount of target cDNA was calculated by comparative threshold (Ct) method and expressed by means of the $2^{-\Delta\Delta Ct}$ method (Livak and Schmittgen, 2012) using the hypoxanthine ribosyltransferase (HPRT1) as an internal control.

2.9. Statistical analysis

Statistic analysis was performed by Graph Pad Prism 5 software. Data are expressed as mean values ± SEM (±SD for DLS) for the indicated number of independent determinations. The statistical significance was calculated by the Student's t-test for time-response experiments. For the MTT assay, spectrofluorimetric endocytosis and real time PCR analysis was performed the one way ANOVA with Bonferroni's multiple comparison test and differences were considered

Table 2
Size, zeta potential values and PdI (polydispersity index) of 44 nm (NP44) and 100 nm (NP100) PS-NPs.

PS-NPs	Medium	Temp °C	Size [nm]	Size [SD]	Size ratio [DMEM/water]	Z-potential [mV]	Z-potential [SD]	PdI	PdI [SD]
NP 44 nm	H_2O	25	49.04 ± 0.5789[a]	1.003	0.951	−35.87 ± 0.3480[a]	0.6028	0.1060 ± 0.01097[a]	0.0190
	DMEM		46.65 ± 0.4495[a]	0.7785		−40.5 ± 0.9539[a]	1.652	0.1333 ± 0.02282[a]	0.03953
	H_2O	37	60.64 ± 0.8398[a]	1.455	0.899	−24.13 ± 0.7219[a]	1.250	0.3047 ± 0.02325[a]	0.04028
	DMEM		54.55 ± 0.8624[a]	1.494		−37.57 ± 0.4631[a]	0.8021	0.2230 ± 0.02730[a]	0.04729
NP 100 nm	H_2O	25	76.31 ± 0.6340[a]	1.098	1.067	−36.33 ± 0.2963[a]	0.5132	0.1850 ± 0.0050[a]	0.008660
	DMEM		81.42 ± 0.332[a]	0.575		−38.47 ± 0.0333[a]	0.005773	0.1657 ± 0.006692[a]	0.01159
	H_2O	37	81.47 ± 0.2949[a]	0.5108	1.070	−36.23 ± 0.8667[a]	1.501	0.1567 ± 0.003180[a]	0.005508
	DMEM		87.23 ± 0.214[a]	0.3707		−34.97 ± 0.6173[a]	1.069	0.1853 ± 0.00441[a]	0.007638

SD: standard deviation a) Mean value ± SE, n = 3.

Table 3
Primers used in qPCR.

Gene	5′-Forward-3′	5′-Reverse-3′
c-Myc	AGGGTCAAGTTGGACAGTGTCA	TGGTGCATTTTCGGTTGTTG
ERK-1	CGCGTGGCCATCAAGAAG	GCGCTGGCAGTAGGTCTGA
Ki67	CCCGTGGGAGACGTGGTA	TTCCCGTGACGCTTCCA
CCNE1	GATGACCGGGTTTACCCAAA	CCTCTGGATGGTGCAATAATCC
CCND1	CGTGGCCTCTAAGATGAAGGA	CGGTGTAGATGCACAGCTTCTC
p38	CACCAGACCTACTGCCAGAGAA	TCTCATGTCTGAAGCGCAGTAAG
p53	TCTGTCCCTTCCCAGAAAACC	CAAGAAGCCCAGACGGAAAC
IL8	CTGGCCGTGGCTCTCTTG	CTTGGCAAAACTGCACCTTCA
IL6	GCTGCAGGCACAGAACCA	GCTGCGCAGAATGAGATGAG
IL1-β	ACGATGCACCTGTACGATCACT	CACCAAGCTTTTTTGCTGTGAGT
TGFβ1	GCCCACTGCTCCTGTGACA	CCGGTAGTGAACCCGTTGAT
NF-kβ1	AAGTGCAGAGGAAACGTCAGAAG	CTACCACCGCCGAAACTATCC
HPTR1	GACTTTGCTTTCCTTGGTCAGGCA	ACAATCCGCCCAAAGGGAACTGA

statistically significant when the P value was at least <0.05. For the distribution of the total number of NPs/μm^2 and the mean number of NPs/μm^2 aggregates inside cells the one way ANOVA Kruskal–Wallis test was performed and P value was considered significant when <0.05. All the experiments were performed in triplicate and repeated at least three times.

3. Results

3.1. PS-NPs characterization

The size, zeta potential and PdI of PS-NPs, after 1 h of incubation with DMEM or H_2O, were probed by DLS.

Table 2 shows that NP44, in water or DMEM have similar dimension; its diameter is slightly higher at 37 °C. NP100 (as declared by the supplier) show, by DLS, a real size of about 80 nm in water and in DMEM for both temperatures tested. The values of PdI and zeta-potential indicate that PS-NPs do not form aggregates in both solutions. The only exception that we observed is relatively to NP44 in water at 37 °C that show a PdI value of 0.3 and a z-potential value of about −24.13 mV, indicating a low level of aggregation.

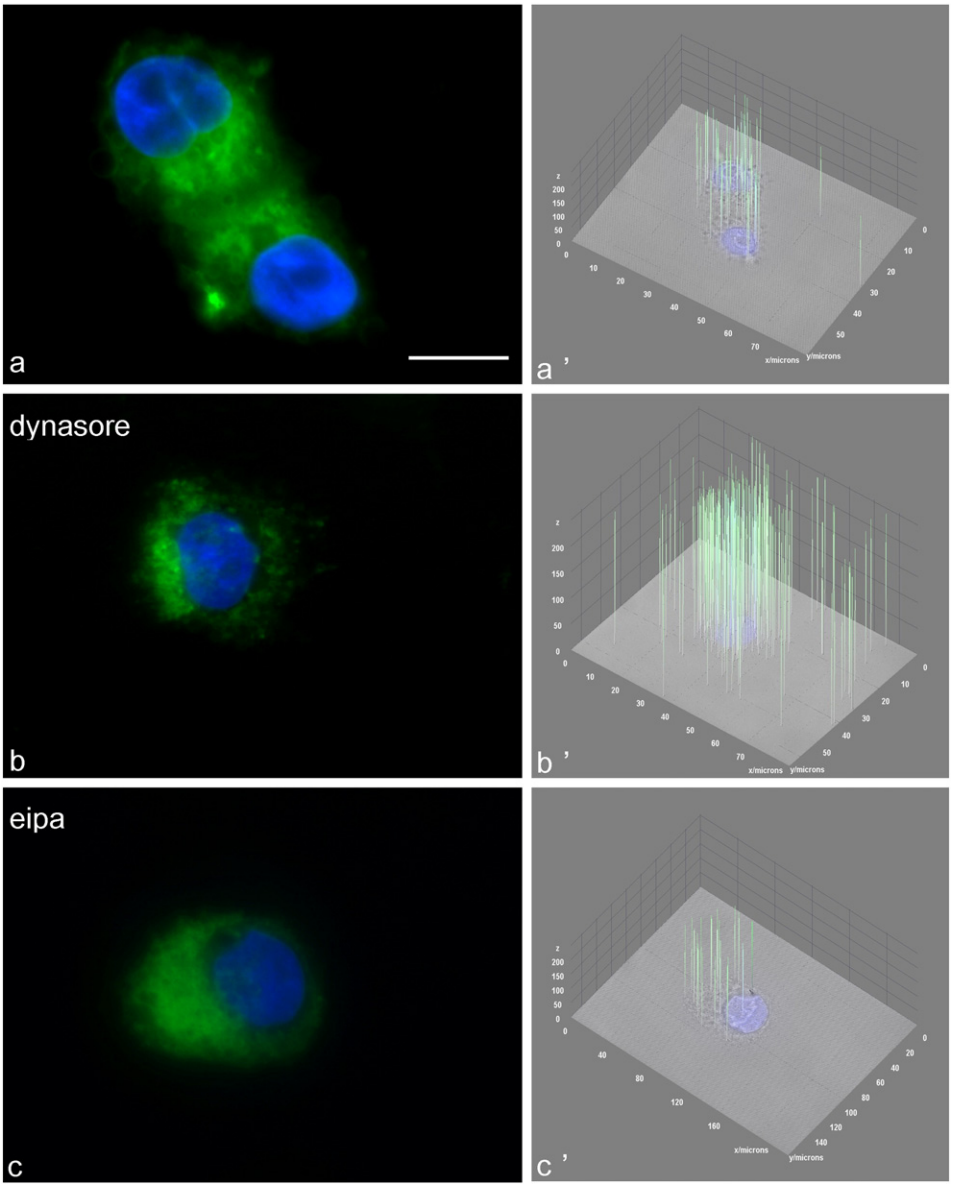

Fig. 1. Uptake of PS-NPs of 44 nm (NP44) by AGS cells. NP44 are labeled with fluorescein isothiocyanate. AGS cells were grown in chamber slides, incubated 1 h with NP44 alone (a) or pre-treated with dynasore (b) or EIPA (c) for 30 min at 37 °C. Following pre-treatment with inhibitor drugs cells were incubated with NP44 for 1 h and analyzed with epifluorescence microscopy. Nuclei were stained with Höechst. The inserts on the right show the intracellular distribution of single or multiple aggregates of PS-NPs after deconvolution process. Scale bar 10 μm.

3.2. Fluorescence microscopy

PS-NPs uptake, with or without inhibitor drugs, was monitored by epifluorescence microscopy (Figs. 1; 2). Experiments performed after 1 h at 37 °C of incubation, without inhibitors, revealed that NP44 and NP100 are able to accumulate in the cytoplasm, without reaching the nucleus (Figs. 1a; 2a); nuclei appeared without any nanoparticles-associated signal. Dynasore and EIPA were used to investigate the endocytic pathways involved in the PS-NPs internalization. The inhibition studies were performed only for 1 h because it has been reported that blocking one route of uptake for longer time might activate other pathways of endocytosis (Conner and Schmid, 2003; Harush-Frenkel et al., 2007). AGS treated with 25.9 μg/ml of dynasore showed fluorescent signal both for NP44 and NP100 (Figs. 1b; 2b); similarly, PS-NPs were found in the cytoplasm of cells treated with EIPA (30 μg/ml) (Figs. 1c; 2c).

3.3. Spectrofluorimetric assays

We performed a spectrofluorimetric analyses in order to evaluate the efficiency of nanoparticles internalization by AGS. Overall the uptake was less than 15% of the PS-NPs administered (Fig. 3). After the cell lysis, intensity of fluorescence was indicative of PS-NPs uptake. As shown in Fig. 3 we observed a low rate of internalization for NP100, despite incubation with 10 μg/ml, with a maximum value reached after 30 min of incubation; NPs accumulate in AGS in a time dependent-manner; however, after 1 h, we found a slight decrease of NP100 internalization. NP44 analysis revealed a fast degree of uptake, even at short times of incubation. The peak of cellular uptake was found after 30 min, with about 1.8 μg/ml of PS-NPs internalized. As for NP100, this value decreased after 1 h (Fig. 3).

Quantitative analyses were performed even at 4 °C and in the presence of inhibitor drugs (Fig. 4); data revealed that pre-incubation

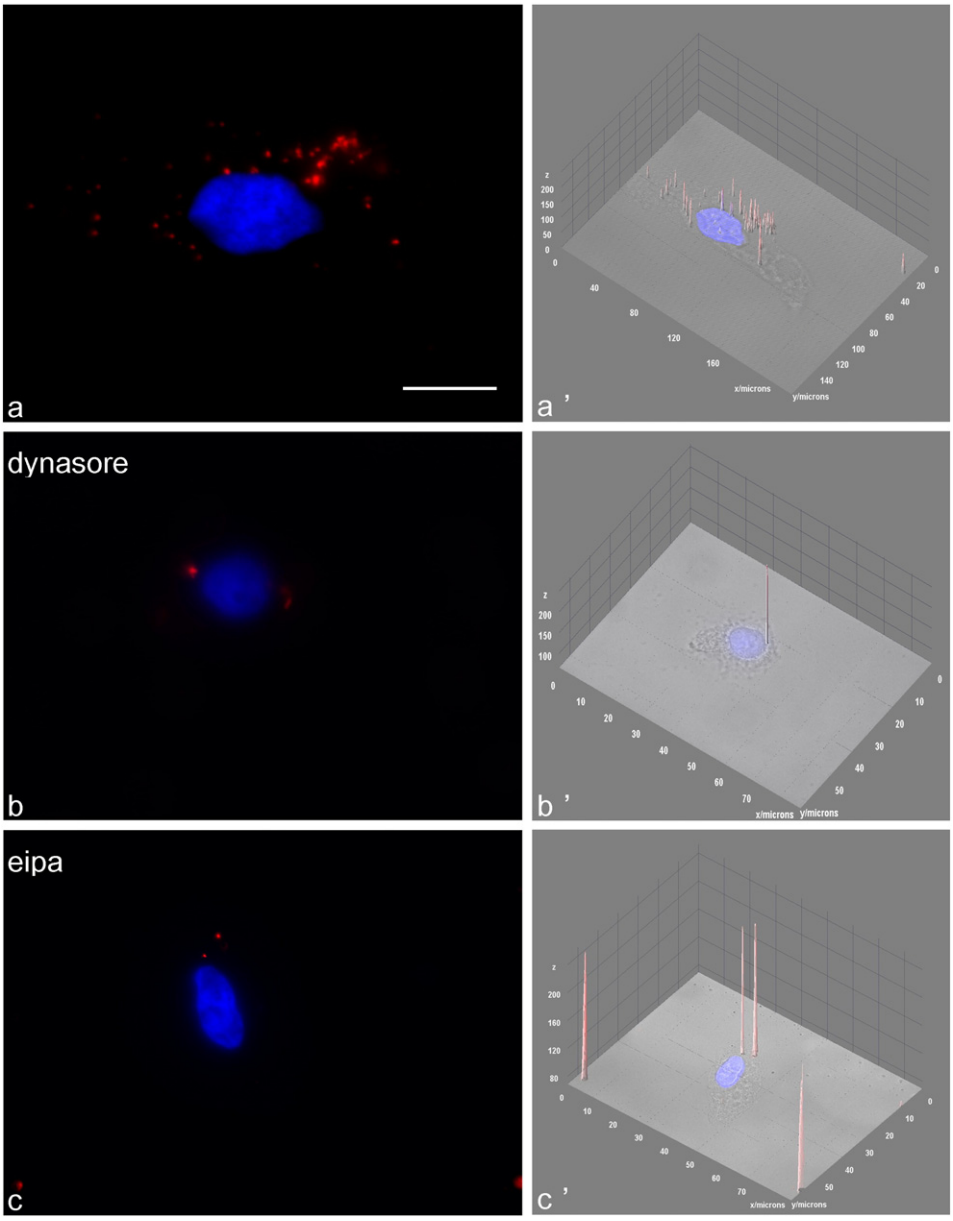

Fig. 2. Uptake of PS-NPs of 100 nm (NP100) by AGS cells. NP100 are labeled with rhodamine. AGS cells were grown in chamber slides, incubated 1 h with NP100 alone (a) or pre-treated with dynasore (b) or EIPA (c) for 30 min at 37 °C. Following pre-treatment with inhibitor drugs cells were incubated with NP100 for 1 h and analyzed with epifluorescence microscopy. Nuclei were stained with Höechst. The inserts on the right show the intracellular distribution of single or multiple aggregates of PS-NPs after deconvolution process. Scale bar 10 μm.

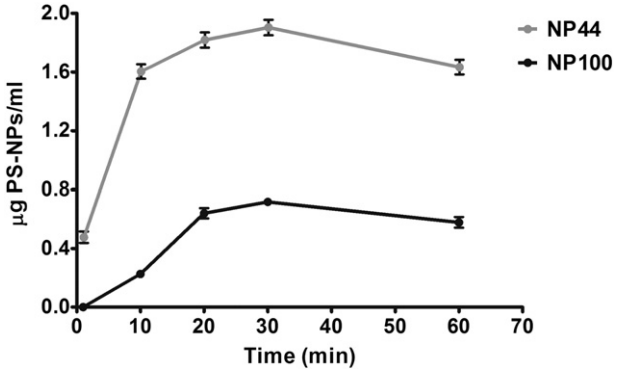

Fig. 3. Spectrofluorimetric analysis of PS-NPs uptake kinetics in AGS cells. NP44 are faster and more efficiently internalized by AGS (1 min) compared to NP100. Both nanoparticles show the highest rate of uptake after 30 min and a plateau between 30 min and 1 h of incubation. The calibration curve has $R^2 = 0.995$ for NP100 and $R^2 = 0.996$ for NP44, respectively. Values are significant for $P < 0.05$.

at 4 °C strongly inhibited PS-NPs internalization, both for NP100 both for NP44; NP100 internalization was affected by treatment with both inhibitor drugs; however, dynasore reduced most notably NP100 uptake if compared with EIPA (Fig. 4b). Dynasore also reduced NP44 internalization. EIPA, instead, didn't affect this uptake, with values comparable with control group (Fig. 4a).

The dose effect experiments showed that the uptake of NP44 was slightly dose dependent, at least for lower concentrations, with an inverse proportionality (Fig. 5a). The percentage of uptake for NP100 was inverse to the concentration with the highest amounts at the lowest administered dose (Fig. 5b). For both PS-NPs the dose experiments confirmed that the efficiency of uptake was about 10–30% but NP100 showed lower uptake efficiency (Fig. 5).

3.4. Image analysis of PS-NPs distribution

Image analyses showed that neither dynasore nor EIPA were able to block NP44 internalization after 1 h of exposure to NP44 (Fig. 6a; c); although a decrease was observed when dynasore or EIPA was used, the total number of NP44/µm^2 and the mean number of NP44/µm^2 aggregates inside cells did not significantly vary (Fig. 6a; c). Conversely, NP100 internalization was blocked by dynasore of about 65% after 1 h of exposure (Fig. 6b; **d**). Surprisingly, EIPA treatment increased the single NP100 internalization during intracellular PS-NPs cluster aggregation; in particular at least doubling the internalization of single NP100 and about six times the internalization of NP100 pairs (Fig. 6b); the mean number of NP100 internalized increased by about 3.6 times the control (Fig. 6d). Furthermore the cluster formation was more prominent in the NP44 treated cells compared to NP100 treated cells (Fig. 6a; b), where PS-NPs formed aggregates of maximum three PS-NPs when EIPA was used (Fig. 6b).

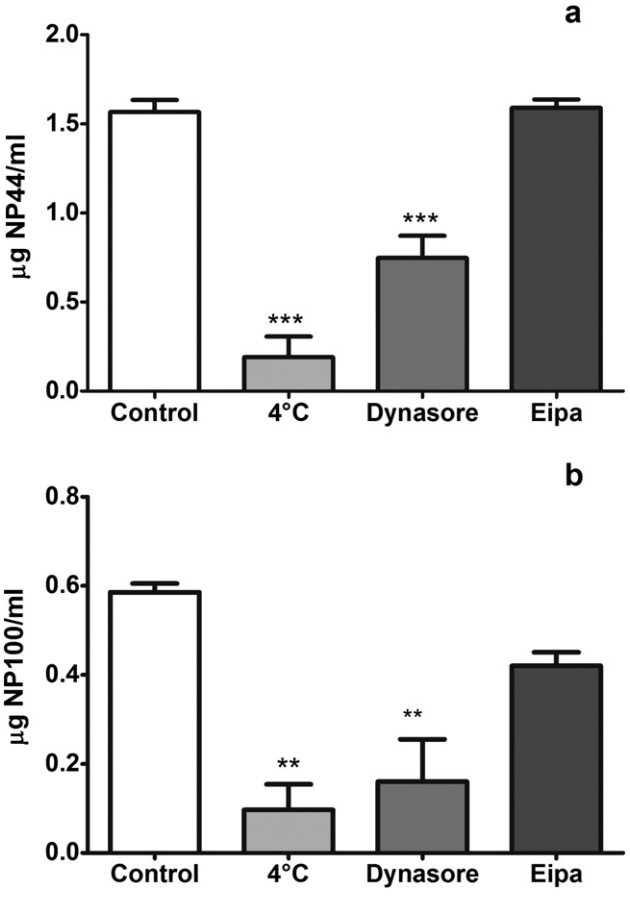

Fig. 4. Inhibitory studies with quantitative spectrofluorimetric analysis. Effects of dynasore, EIPA, and 4 °C treatments on NP44 (a) and NP100 (b) uptake: the cells were 30 min pre-treated with inhibitor drugs or pre-incubated at 4 °C and then 1 h incubated with PS-NPs. $^{**}P < 0.01$, $^{***}P < 0.001$ related to control group.

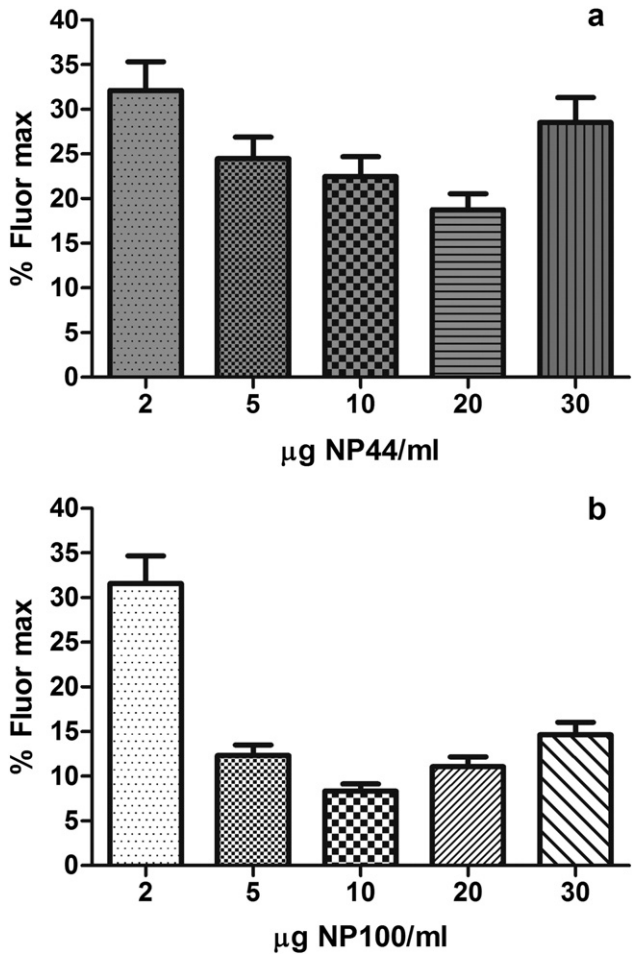

Fig. 5. Quantitative spectrofluorimetric assay. Concentration response of PS-NPs treatment on AGS cells, after 1 h treatment with NP44 (a) and NP100 (b). The uptake is not dependent by the administrated concentration of PS-NPs.

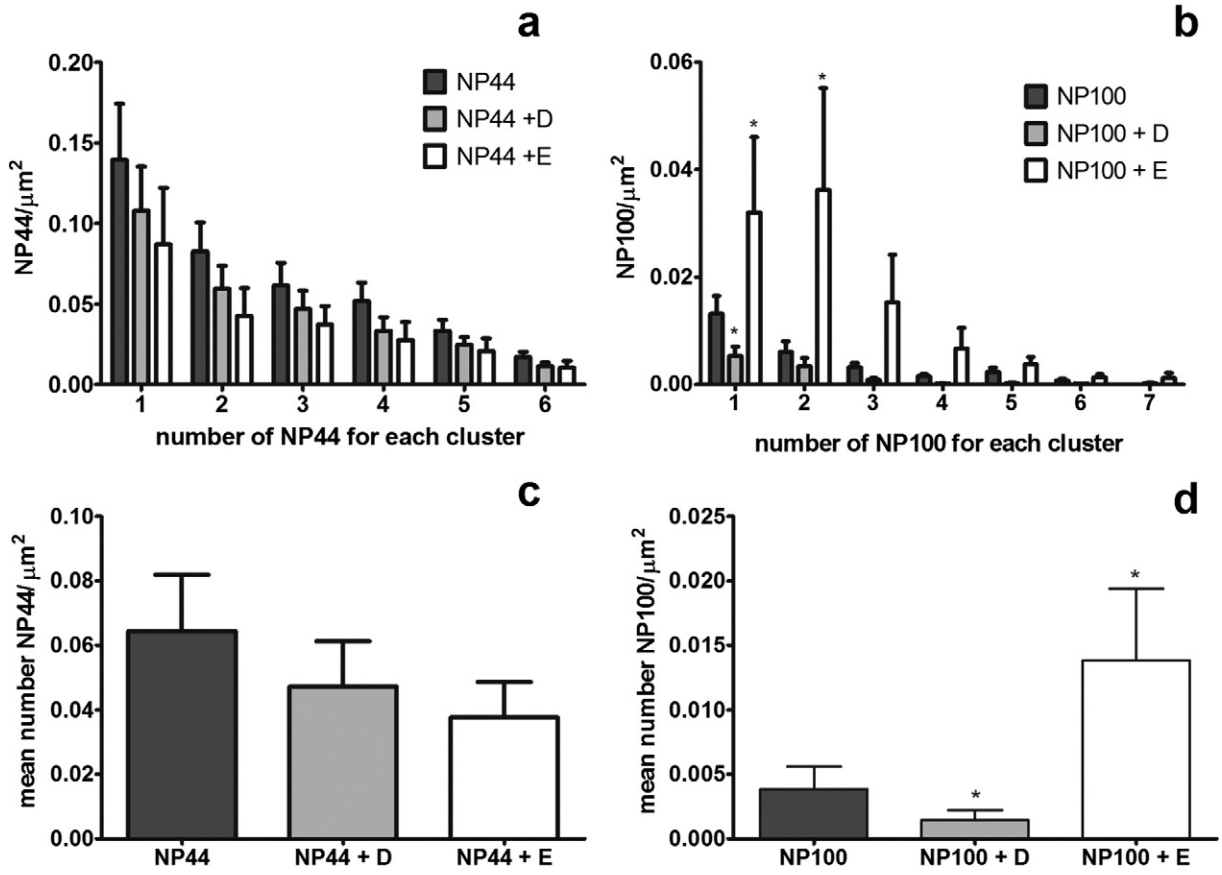

Fig. 6. Image analysis for intracellular detection of PS-NPs after endocytosis or macropinocytosis/phagocytosis inhibition, NPs internalization on AGS cells (n = 100 cells for each experimental class). Neither dynasore (+D) nor EIPA (+E) are able to significantly block NP44 internalization after 1 h of exposure to NP44 as reported by the total number of NP44/μm^2 and the mean number of NP44/μm^2 clusters inside cells which did not vary significantly (a, c). NP100 internalization was blocked by dynasore of about 65% after 1 h of exposure (*P < 0.05) (b). EIPA treatment increases the NP100 intracytoplasmic accumulation, in particular at least doubling the internalization of single NP100 and about six times the internalization of NP100 pairs (*P < 0.05) (b); the mean number of NP100 internalized increases of about 3.6 times the control (*P < 0.05) (d).

3.5. Morphological investigation

The potential toxic effect of PS-NPs may also be indicated by morphological alteration of the cells. Hence we investigated the morphology of cells after exposure to PS-NPs using the fluorescence microscope and Höechst staining.

After NPs exposure for 1 h, there was a morphological change in the nucleus/cytoplasm area ratio, due mainly to an enlargement of cytoplasm in the PS-NPs treated cells (Fig. 7). No differences in nucleus morphology were observed (data not showed).

3.6. Cell viability assay

NP100 and NP44 were tested for the possibility to alter the viability of AGS. To perform the experiments, increasing concentrations of PS-NPs were added to AGS cells and cell viability after 24 h was measured using the MTT assay. Results from both PS-NPs were similar for lowest concentrations (1 μg/ml and 2 μg/ml) and showed no effects (Fig. 8a; b). However, concentration of 10 μg/ml affected cell viability; for NP100 viability was significantly stimulated (Fig. 8b) while NP44 decreased the number of viable cells (Fig. 8a).

3.7. Real time PCR

Quantitative RT-PCR for AGS control and treated for 1 h with each class of PS-NPs (NP44 and NP100) revealed that the evaluated transcripts were expressed in all three experimental classes. The mRNA levels were normalized against the levels of hypoxanthine ribosyltransferase (HPRT1) housekeeping gene. For the genes involved in proliferation pathways ERK1, CCNE1 (coding for cyclin E), CCND1 (coding for cyclin D) no significant variation of the levels of their respective transcripts was observed. However, a down-regulation of Ki67 gene expression was observed in AGS treated with both types of PS-NPs, while only NP44 weakly increased c-Myc mRNA levels. Both sizes of nanoparticles weakly changed the levels of NF-kβ1 and TGF1β mRNA. Pro-inflammatory cytokine genes IL1β, IL6 and IL8 were up-regulated by both PS-NPs. In particular, increasing in mRNA levels for IL6 and IL8 was about 7 fold higher than control in NP44 treated cells (Fig. 9).

4. Discussion

Nanoparticles are receiving more and more attention from scientific community due to their wide potential, especially in nanomedicine, both in diagnosis and therapy. For example, it has been suggested that the optimal NPs diameter in molecular imaging ranging between 30 and 150 nm, thus also permitting to use them as cargoes of numerous molecules within each nanoparticle (Debbage and Jaschke, 2008). Moreover a number of clues suggest that PS-NPs, as product of plastic environmental degradation, may affect the food chain, rising concerns about food safety (Mattsson et al., 2014; Shang et al., 2014). In this perspective, information about their interactions with cells, in terms of toxicity or cellular uptake is still controversial and far from being elucidated. For these reasons, we decided to study the effects of PS-NPs of two different sizes (44 nm and 100 nm) on human gastric

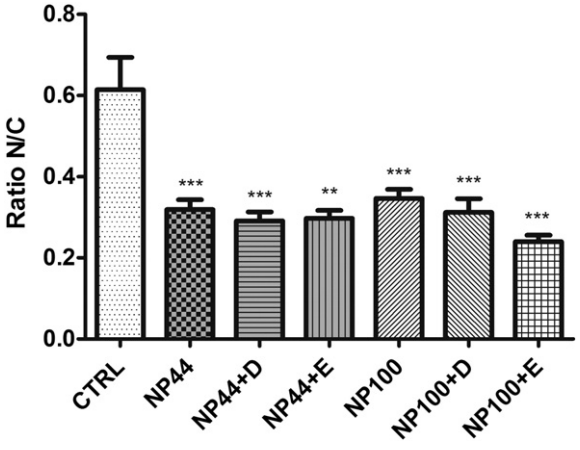

Fig. 7. Ratio nucleus/cytoplasm (N/C) of AGS cells. Cells were treated for 1 h with PS-NPs alone or in combination with inhibitor drugs (+D: dynasore; +E: EIPA). Values are significant for $^{**}P < 0.01$ and $^{***}P < 0.001$ related to control group.

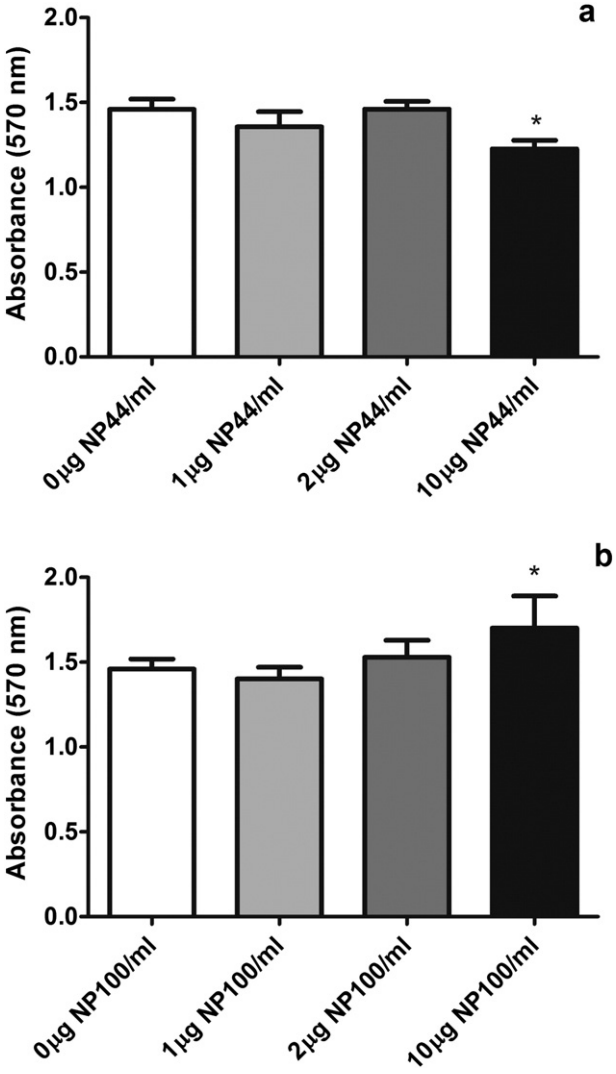

Fig. 8. Cell viability assay after PS-NPs incubation. AGS cells were exposed for 24 h to different concentrations of NP44 (a) and NP100 (b). Cell viability was determinate by MTT assay. At the highest concentration (10 µg/ml), NP44 and NP100 inhibited and stimulated cell viability, respectively. $^{*}P < 0.05$ related to control group (0 µg/ml).

adenocarcinoma (AGS) cells, investigating their kinetics and pathways of internalization, viability and gene expression. The DLS analysis confirms the dimensions of NP44 but these NPs show a low level of aggregation at 37 °C. In contrast NP100 show a diameter of about 80 nm both in H_2O and in DMEM. PS-NPs do not aggregate in water or in the medium used in the experimental conditions both at 25 and 37 °C. Our data suggest that both PS-NPs we used are suitable for uptake studies. The first data is that PS-NPs are internalized by AGS, although with different kinetics and different efficiencies; NP44 quickly enter in the cytoplasm and reach the highest amount after 30 min of incubation; in contrast, NP100 always show a lower and slower degree of internalization; this is consistent with the thesis that smaller size facilitates cellular PS-NPs uptake (Debbage and Jaschke, 2008). Interestingly, both NP44 and NP100 show saturable internalization after 1 h of treatment: we hypothesize that when AGS cells become saturated by NPs, a release process may be activated, as shown in literature (Iversen et al., 2011). It is noteworthy that the PS-NPs uptake is slightly dose dependent for smaller PS-NPs, with an inverse proportionality; this latter feature is accentuated for larger PS-NPs. This could be due to the saturable kinetic of PS-NPs uptake and is consistent with the time dependent profile of their internalization, suggesting that a non-passive uptake occurs. As a consequence, we studied the endocytic pathway of PS-NPs internalization. Although Salvati et al. (2011) demonstrated that temperature is not a limiting factor for PS-NPs uptake, our low temperature experiments demonstrate that uptake of PS-NPs is an energy dependent process and not a mechanism of passive translocation through the cell membrane (i.e. simple or facilitated diffusion). This is relevant to the human gastric cell physiology and toxicology as the gastrointestinal tract is one of the major pathways of exposure for environmental contaminants of food and water and for many pharmaceuticals. NPs that are internalized by passive transport may not show a target specificity accumulating inside cells only on the basis of size, concentration gradient, lipid solubility and electrical charge, as other environmental contaminants do. This may dramatically alter the cell homeostasis, with a maximum adsorption in the cell that may be the cause of toxicity and deleterious effects (Kent, 1998). Hence, the absence of internalization at 4 °C suggests that other mechanisms are involved in the PS-NPs internalization. Inhibition studies were performed for 1 h as mentioned above, with dynasore and EIPA, in order to inhibit clathrin dependent endocytosis and macropinocytosis/phagocytosis, respectively. The high inhibitory effect of dynasore on PS-NPs uptake demonstrates that PS-NPs of both sizes are internalized predominantly through the endocytic/caveolin compartments. Conversely, the lack of inhibition of the treatment with EIPA shows that macropinocytosis/phagocytosis is not involved in the internalization of PS-NPs, thus confirming the time- and dose-dependent PS-NPs uptake profile. Performing the fluorescence image analysis we determined the number of PS-NPs clusters in the fluorescent portion of the AGS cells; we showed that NP44 are accumulated in the AGS cytoplasm in higher amounts than NP100. We also demonstrated that the accumulation of NP44 in the cytoplasm is carried out in single or low number without any preference (maximum 6 nanoparticles/cluster). Considering NP100, our data show that the low amount of NP100 is internalized preferably in low number of PS-NPs for each cluster (1–2 nanoparticle/cluster). Moreover, the treatment with dynasore or EIPA alters the internalization pathway of both sizes of PS-NPs, roughly confirming the bulk of spectrofluorimetry results, although, surprisingly, EIPA seems to enhance the clusterization of NP100. Notwithstanding the cause of this result remains to be establish, this may be speculatively explained in several ways: the size of internalized PS-NPs clusters can be linked to the endocytic vesicles which are about 200 nm large thus EIPA treatment can improve different internalization processes like endocytosis; otherwise the previously reported action of EIPA on actin filaments disarrangement may be an explanation (Ivanov, 2003). Thus our results confirm that clathrin mediated endocytosis is the privileged endocytic pathway during internalization as

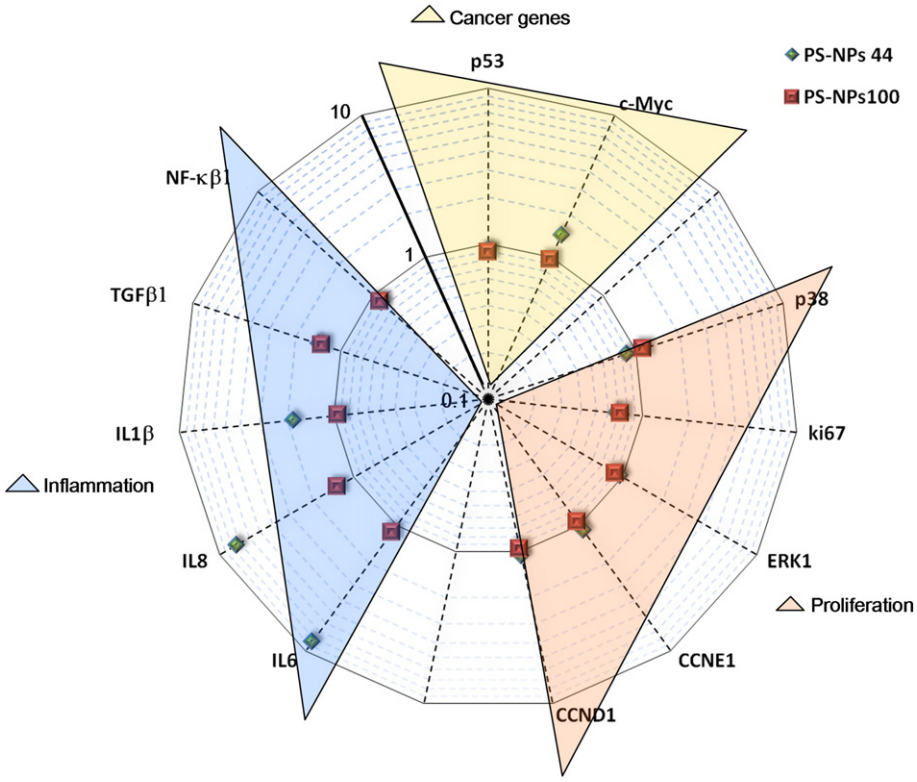

Fig. 9. Gene expression analysis with qPCR. PS-NPs administration determines alteration of gene expression in AGS cells, as shown by logarithmic chart of qPCR experiments. NP44 increase the expression of the inflammatory pathway. The distance from the first circular line indicates the fold-change from the control which is normalized to 1 (Significant values: NP44: $P < 0.001$ IL1β, TGFβ1, IL8, cMyc, Ki67; $P < 0.01$ NF-kβ1, IL6; $P < 0.05$ p38; NP100: $P < 0.001$ TGFβ1, Ki67; $P < 0.01$ NF-κβ1; $P < 0.05$ p38).

reported in literature for other NPs of the same dimension range (Lai et al., 2007; Rejman et al., 2004) and in addition suggest that other pathways are involved. After demonstrating the cellular uptake, we investigated the biological effects caused by PS-NPs in AGS cells. The cytomorphologic investigation evidenced changes in the nucleus/cytoplasm ratio after PS-NPs treatment; PS-NPs treated cells appear with engulfed and enlarged cytoplasm compared to controls, resulting in a consistent decrease of the nucleus/cytoplasm ratio. The alteration of the nucleus to cytoplasmic ratio is often reported as a clear signal of carcinoma abnormalities (Idowu and Powers, 2010) and as the effect of the accumulation of exogenous material in the cytoplasm (Savagner and Landes, 2005). Furthermore, during the *Helicobacter pylori* infection of AGS, the spreading of cell contours had previously been reported (Segal et al., 1999). Hence, cytomorphological features of PS-NPs-treated AGS cells may suggest that PS-NPs can alter the phenotype of gastric cancer cells as other *in vivo* tumor or inflammatory agents do. Using different concentrations of PS-NPs we demonstrated that at lower concentration, PS-NPs do not affect cell viability, while at the highest concentration the cell viability is affected in a size dependent manner; NP44 inhibit cell viability and NP 100 stimulate cell viability; about cell viability, other studies reported size-dependent effects on both for non-polystyrene nanoparticles and for PS-NPs (Oh et al., 2010; Jin et al., 2008). This size-dependent opposite effect on AGS cell viability is possibly due to the higher and faster uptake of smaller PS-NPs which correspond to a pervasive internalization. Our data demonstrate that not every size of PS-NPs is suitable for medical application, suggesting that size is a basic parameter to consider for toxicology strategy against cancer, with smaller size PS-NPs possibly useful in anti-proliferative cancer treatment. Through qPCR analysis we investigated several genes involved in inflammation and proliferation processes. Our data revealed that in NP44 AGS treated cells pro-inflammatory cytokines IL6, IL8 and IL1β genes are up-regulated, IL6 and IL8 showing the highest fold-change in mRNA levels. IL6 and IL8, as well as IL1β are well known pro-inflammatory cytokines involved in gastric pathology, including gastric carcinogenesis (Kinoshita et al., 2013; Macrì et al., 2006; Yamada et al., 2013). In literature, IL6 and IL8 are reported to be over-expressed in *H. pilori* infection (Alzahrani et al., 2014; Lee et al., 2013) and their over-expression is considered as the first step for the development of gastric cancer, both *H. pilori* dependent and not (Asfaha et al., 2013; Kido et al., 2001; Kim et al., 2003; Lee et al., 2004). Moreover, both PS-NPs increase TGF1β mRNA levels which evokes both pro-inflammatory and anti-inflammatory responses in gastric cells (Hong et al., 2010). Thus, NP44 act as an inflammatory agent. This response seems to be linked to an anti-proliferative effect and is in accordance with our results of MTT assay and Ki67 and NF-kβ1 down-regulation. The induction of c-Myc does not seem to balance this anti-proliferative effect. However, since the expression of p53 does not change and nuclear appearance is normal and not fragmented, apoptosis may be excluded, suggesting a fast onset of a stress response. Considering NP100, they weakly affect proliferation genes (increasing p38 and decreasing p53 and Ki67), with a null effect on interleukins, but produce an increase of TGF1β and a decrease of NF-kβ1. However, NP100 increase cell viability but concomitantly Ki67 mRNA decreases thus suggesting that the NP100 induced-metabolic activation is not associated to an increase in proliferation. This is consistent with a general lower effect of NP100 on AGS cells compared to NP44, as showed by their uptake profile and kinetic of internalization. In conclusion, in this study we have shown that AGS cells internalize PS-NPs in size, concentration and time-dependent manner; PS-NPs are internalized by predominantly clathrin-mediated endocytosis, although other pathways may be involved; PS-NPs undergo a release process after 1 h of interaction with cells. Moreover, when internalized, PS-NPs are able to affect gene expression, resulting in inflammatory responses and morphological alterations, especially when those of smaller size were used. Even if

other studies are necessary to determine the risk factors associated to PS-NPs uptake, our data suggest that the NPs use is a double side story: while smaller PS-NPs may be useful in anticancer treatment, careful attention must be taken when larger NPs are chosen as cargoes for nanomedicine, also rising concerns about their safety for human gastric adsorption through the food chain.

Transparency document

The Transparency document associated with this article can be found, in online version.

Acknowledgements

This work was supported by University of Naples Federico II (Programma FARO, Finanziamento per l'Avvio di Ricerche Originali). We thank Prof. Robin Lindsay for helping in English Language.

References

Alzahrani, S., Lina, T.T., Gonzalez, J., Pinchuk, I.V., Beswick, E.J., Reyes, V.E., 2014. Effect of *Helicobacter pylori* on gastric epithelial cells. World J. Gastroenterol. 20, 12767–12780.

Asfaha, S., Dubeykovskiy, A.N., Tomita, H., et al., 2013. Mice that express human interleukin-8 have increased mobilization of immature myeloid cells, which exacerbates inflammation and accelerates colon carcinogenesis. Gastroenterology 144, 155–166.

Bareford, L.M., Swaan, P.W., 2007. Endocytic mechanisms for targeted drug delivery. Adv. Drug Deliv. 59, 748–758.

Beer, C., Foldbjerg, R., Hayashi, Y., Sutherland, D.S., Autrup, H., 2012. Toxicity of silver nanoparticles — nanoparticle or silver ion? Toxicol. Lett. 208, 286–292.

Boczkowski, J., Hoet, P., 2010. What's new in nanotoxicology? Implications for public health from a brief review of the 2008 literature. Nanotoxicology 4, 1–14.

Boraschi, D., Costantino, L., Italiani, P., 2012. Interaction of nanoparticles with immunocompetent cells: nanosafety considerations. Nanomedicine (Lond.) 7, 121–131.

Cai, X.J., Xu, J.J., 2011. Nanomaterials in controlled drug release. Cytotechnology 63, 319–323.

Cedervall, T., Hansson, L.A., Lard, M., Frohm, B., Linse, S., 2012. Food chain transport of nanoparticles affects behaviour and fat metabolism in fish. PLoS One 7 (2), e32254.

Conner, S.D., Schmid, S.L., 2003. Regulated portals of entry into the cell. Nature 422, 37–44.

Cuenca, A.G., Jiang, H., Hochwald, S.N., Delano, M., Cance, W.G., Grobmyer, S.R., 2006. Emerging implications of nanotechnology on cancer diagnostics and therapeutics. Cancer 107, 459–466.

Daunsend, J., Musyanovych, A., Dass, M., et al., 2008. Uptake mechanism of oppositely charged fluorescent nanoparticles in HeLa cells. Macromol. Biosci. 8, 1135–1143.

Debbage, P., Jaschke, W., 2008. Molecular imaging with nanoparticles: giant roles for dwarf actors. Histochem. Cell. Biol. 130, 845–875.

Dekkers, S., Krystek, P., Peters, R.J.B., Lankveld, et al., 2011. Presence and risks of nanosilica in food products. Nanotoxicology 5, 393–405.

Ferrari, M., 2005. Cancer nanotechnology: opportunities and challenges. Nat. Rev. Cancer 5, 161–171.

Fröhlich, E., Meindl, C., Roblegg, E., Ebner, B., Absenger, M., Pieber, T.R., 2012. Action of polystyrene nanoparticles of different sizes on lysosomal function and integrity. Part. Fibre Toxicol. 12 (9) 26 (Jul). http://dx.doi.org/10.1186/1743-8977-9-26.

Gagnon, E., Duclos, S., Rondeau, C., Cehevet, E., Cameron, P.H., et al., 2002. Endoplasmic reticulum-mediated phagocytosis is a mechanism of entry into macrophages. Cell 110, 119–131.

Geys, J., Coenegrachts, L., Vercammen, J., Engelborghs, Y., Nemmar, A., Nemery, B., Hoet, P.H.M., 2006. In vitro study of the pulmonary translocation of nanoparticles: a preliminary study. Toxicol. Lett. 160, 218–226.

Guarnieri, D., Guaccio, A., Fusco, S., Netti, P.A., 2011. Effect of serum proteins on polystyrene nanoparticle uptake and intracellular trafficking in endothelial cells. J. Nanopart. Res. 13, 4295–4309.

Harush-Frenkel, O., Debotton, N., Benita, S., Altschuler, Y., 2007. Targeting of nanoparticles to the clathrin-mediated endocytic pathway. Biochem. Biophys. Res. Commun. 353, 26–32.

Holzapfel, V., Musyanovych, A., Landfester, K., Lorenz, M.R., Mailander, V., 2005. Preparation of fluorescent carboxyl and amino functionalized polystyrene particles by miniemulsion polymerization as markers for cells. Macromol. Chem. Phys. 206, 2440–2449.

Hong, S., Lee, H.J., Kim, S.J., Hahm, K.B., 2010. Connection between inflammation and carcinogenesis in gastrointestinal tract: focus on TGF-beta signaling. World J. Gastroenterol. 16, 2080–2093.

Idowu, M.O., Powers, C.N., 2010. Lung cancer cytology: potential pitfalls and mimics — a review. Int. J. Clin. Exp. Pathol. 3, 367–385.

Ivanov, A.I., 2003. Pharmacological inhibition of endocytic pathways: is it specific enough to be useful? Methods Mol. Biol. 15-33.

Iversen, T.G., Skotland, T., Sandvig, K., 2011. Endocytosis and intracellular transport of nanoparticles: present knowledge and need for future studies. NanoToday 6, 176–185.

Jin, et al., 2008. Nanoelectronics Conference. INEC 2008. 2nd IEEE International, 24–27 March 2008, pp. 1087–1092.

Johnston, H.J., Semmler-Behnke, M., Brown, D.M., Kreyling, W., Tran, L., Stone, V., 2010. Evaluating the uptake and intracellular fate of polystyrene nanoparticles by primary and hepatocyte cell lines in vitro. Toxicol. Appl. Pharmacol. 242, 66–78.

Kent, C., 1998. Basics of Toxicology. ISBN: 978–0-471-29982-0

Kido, S., Kitadai, Y., Hattori, N., Haruma, K., Kido, T., Ohta, M., et al., 2001. Interleukin 8 and vascular endothelial growth factor—prognostic factors in human gastric carcinomas? Eur. J. Cancer 37, 1482–1487.

Kim, H.K., Song, K.S., Park, Y.S., et al., 2003. Elevated levels of circulating platelet microparticles, VEGF, IL-6 and RANTES in patients with gastric cancer: possible role of a metastasis predictor. Eur. J. Cancer 39, 184–191.

Kinoshita, H., Hirata, Y., Nakagawa, H., Sakamoto, K., et al., 2013. Interleukin-6 mediates epithelial–stromal interactions and promotes gastric tumorigenesis. PLoS One 8, e60914. http://dx.doi.org/10.1371/journal.pone.0060914.

Kirchhausen, T., Macia, E., Pelish, H.E., 2008. Use of dynasore, the small molecule inhibitor of dynamin, in the regulation of endocytosis. Methods Enzymol. 438, 77–93.

Lagana, A., Vadnais, J., Le, P.U., et al., 2000. Regulation of the formation of tumor cell pseudopodia by the Na+/H+ exchanger NHE1. J. Cell Sci. 113, 3649–3662.

Lai, S.K., Kaoru, H., Man, S.T., et al., 2007. Privileged delivery of polymer nanoparticles to the perinuclear region live cells via a non-clathrin, non-degradative pathway. Biomaterials 28, 2876–2884.

Lee, K.H., Bae, S.H., Lee, J.L., Hyun, M.S., Kim, S.H., Song, S.K., Kim, H.S., 2004. Relationship between urokinase-type plasminogen receptor, interleukin-8 gene expression and clinic pathological features in gastric cancer. Oncology 66, 210–217.

Lee, K.E., Khoi, P.N., Xia, Y., Park, J.S., Joo, Y.E., Kim, K.K., Choi, S.Y., Jung, Y.D., 2013. *Helicobacter pylori* and interleukin-8 in gastric cancer. World J. Gastroenterol. 19 (45), 8192–8202.

Livak, K.J., Schmittgen, T.D., 2012. Analysis of relative gene expression data using real time quantitative PCR and the $2^{-\Delta\Delta Ct}$ method. Methods 25, 402–408.

Lunov, O., Syrovets, T., Loos, C., Beil, J., Delacher, M., Tron, K., Nienhaus, G.U., Musyanovych, A., Mailänder, V., Landfester, K., Summet, T., 2011. Differential uptake of functionalized polystyrene nanoparticles by human macrophages and a monocytic cell line. ACS Nano. 5, 1657–1669.

Macia, E., Ehrlich, M., Massol, R., Boucrot, E., Brunner, C., Kirchhausen, T., 2006. Dynasore, a cell-permeable inhibitor of dynamin. Dev. Cell 10, 839–850.

Macrì, A., Versaci, A., Loddo, S., Scuderi, G., Travagliante, M., Trimarchi, G., Teti, D., Famulari, C., 2006. Serum levels of interleukin 1beta, interleukin 8 and tumour necrosis factor alpha as markers of gastric cancer. Biomarkers 11, 184–193.

Mattsson, K., Ekvall, M.T., Hansson, L.A., Linse, S., Malmendal, A., Cedervall, T., 2014. Altered behavior, physiology and metabolism in fish exposed to polystyrene nanoparticles. Environ. Sci. Technol. 49, 553–561.

Mercer, J., Helenius, A., 2009. Virus entry by macropinocytosis. Nat. Cell Biol. 11, 510–520.

Mora-Huertas, C.E., Fessi, H., Elaissari, A., 2010. Polymer-based nanocapsules for drug delivery. Int. J. Pharm. 385, 113–142.

Musyanovych, A., Rossmanith, R., Tontsch, C., Landfester, K., 2007. Effect of hydrophilic comonomer and surfactant type on the colloidal stability and size distribution of carboxyland amino-functionalized polystyrene particles prepared by miniemulsion polymerization. Langmuir 23, 5367–5376.

Nowack, B., Bucheli, T.D., 2007. Occurrence, behavior and effects of nanoparticles in the environment. Environ. Pollut. 150, 5–22.

Oh, W.K., Kim, S., Choi, M., Kim, C., Jeong, Y.S., Cho, B.R., Hahn, J.S., Jang, J., 2010. Cellular uptake, cytotoxicity, and innate immune response of silica–titania hollow nanoparticles based on size and surface functionality. ACS Nano 4, 5301–5313.

Osmond, M.J., McCall, M.J., 2010. Zinc oxide nanoparticles in modern sunscreens: an analysis of potential exposure and hazard. Nanotoxicology 4, 15–41.

Panyam, J., Labhasetwara, V., 2003. Biodegradable nanoparticles for drug and gene delivery to cells and tissue. Adv. Drug Deliv. Rev. 55, 329–347.

Rejman, J., Oberle, V., Zuhorn, I.S., Hoekstra, D., 2004. Size-dependent internalization of particles via the pathways of clathrin- and caveolae-mediated endocytosis. Biochem. J. 377, 159–169.

Salvati, A., Aberg, C., dos Santos, T., Varela, J., Pinto, P., Lynch, I., Dawson, K.A., 2011. Experimental and theoretical comparison of intracellular import of polymeric nanoparticles and small molecules: toward models of uptake kinetics. Nanomedicine 7, 818–826.

dos Santos, T., Varela, J., Lynch, I., Salvati, A., Dawson, K.A., 2011. Effects of transport inhibitors on the cellular uptake of carboxylated polystyrene nanoparticles in different cell lines. Plos One 6, e24438.

Savagner, E.P., Landes, 2005. Rise and Fall of Epithelial Phenotype: Concepts of Epithelial–Mesenchymal Transition. Kluwer Dual Imprint/Landes series: Molecular Biology Intelligence Unit.

Schlorf, T., Meincke, M., Kossel, E., Gluer, C.C., Jansen, O., Mentlein, R., 2011. Biological properties of iron oxide nanoparticles for cellular and molecular magnetic resonance imaging. Int. J. Mol. Sci. 12, 12–23.

Segal, E.D., Cha, J., Lo, J., Falkow, S., Tompkins, L.S., 1999. Altered states: involvement of phosphorylated CagA in the induction of host cellular growth changes by *Helicobacter pylori*. PNAS 96, 14559–14564.

Shang, L., Nienhaus, K., Nienhaus, G.U., 2014. Engineered nanoparticles interacting with cells: size matters. J. Nanobiotechnol. 12, 5.

Smith, P.J., Giroud, M., Wiggins, H.L., et al., 2012. Cellular entry of nanoparticles via serum sensitive clathrin-mediated endocytosis, and plasma membrane permeabilization. Int. J. Nanomed. 7, 2045–2055.

Soriano, J., Villanueva, A., Stockert, J.C., Cañete, M., 2013. Vehiculization determines the endocytic internalization mechanism of Zn(II)-phthalocyanine. Histochem. Cell. Biol. 139, 149–160.
Varela, J.U., Bexiga, M.G., Åberg, C., Simpson, J.C., Dawson, K.A., 2012. Quantifying size-dependent interactions between fluorescently labeled polystyrene nanoparticles and mammalian cells. J. Nanobiotechnol. 3155, 10–39.
Vonesch, C., Unser, M., 2008. A fast thresholded Landweber algorithm for wavelet-regularized multidimensional deconvolution. IEEE Trans. Image Process. 17, 539–549.
Wickline, S.A., Lanza, G.M., 2003. Nanotechnology for molecular imaging and targeted therapy. Circulation 107, 1092–1095.
Xia, T., Kovochich, M., Liong, M., Zink, J.I., Nel, A.E., 2008. Cationic polystyrene nanosphere toxicity depends on cell-specific endocytic and mitochondrial injury pathways. ACS Nano 2, 85–96.
Xiao, L., Xiong, X., Sun, X., Zhu, Y., Yang, H., Chen, H., Gan, L., Xu, H., Yang, X., 2011. Role of cellular uptake in the reversal of multidrug resistance by PEG-b-PLA polymeric micelles. Biomaterials 32, 5148–5157.
Yamada, S., Kato, S., Matsuhisa, T., Makonkawkeyoon, L., et al., 2013. Predominant mucosal IL-8 mRNA expression in non-cagA Thais is risk for gastric cancer. World J. Gastroenterol. 19, 2941–2949.